

Post-print version of:

Publisher: **SAGE**

Journal paper: **Journal of Strain Analysis for Engineering Design 2010, 45(4) 301-318**

Title: **A procedure for evaluating high residual stresses using the blind hole drilling method, including the effect of plasticity**

Authors: **M. Beghini, L. Bertini, C. Santus**

Creative Commons Attribution Non-Commercial No Derivatives License



DOI Link: <https://doi.org/10.1243/03093247JSA579>

# **A procedure for evaluating high residual stresses by the blind hole drilling method including the effect of plasticity**

M. Beghini<sup>a</sup>, L. Bertini<sup>a</sup>, C. Santus<sup>a\*</sup>

<sup>a</sup> Dipartimento di Ingegneria Meccanica Nucleare e della Produzione. Università di Pisa.  
Largo Lucio Lazzarino, n.2 – 56122 – Pisa, Italy.

## **Abstract**

When the blind hole drilling method is used to evaluate high residual stresses in a metallic component, plastic relaxed strain can be produced in the hole region because of the stress concentration that causes the local stresses to reach yielding. By assuming a linear–elastic behavior of the material, a significant error can result. The present paper analyzes the phenomenon of the plasticity locally induced by the introduction of the hole and proposes a procedure to take into account its effects on the residual stress evaluation. The correcting procedure has been developed by elaborating a large database of elastic–plastic Finite Element analyses performed considering a wide range of material properties and testing parameters, including all the strain gage rosettes commonly used. As plasticity induces nonlinearity in the relationship between residual stress and relaxed strain, the superposition principle cannot be applied so the correction is limited to uniform in depth residual stress fields. However, four hole depths were considered and the related correcting procedures were provided. When variable through thickness residual stress is expected, and high residual stress is confined near the surface region, the correction procedure can be applied to an initial limited depth.

## **Keywords**

Blind hole drilling method. Plasticity effect. Correction procedure. Finite element analysis.

---

\*Corresponding author: **Ciro SANTUS**  
ph.: +39 050 2218007; fax: +39 050 2218065  
e-mail: [ciro.santus@ing.unipi.it](mailto:ciro.santus@ing.unipi.it)

## Nomenclature

$D$	Diameter of the gage circle.
$G_L$	Gage length.
$G_W$	Gage width.
$D_0$	Diameter of the drilled hole.
$\delta = D_0/D$	Ratio between gage circle and drilled hole diameters.
$Z$	Hole depth.
$H$	Specimen thickness.
$\sigma_x, \sigma_y$	Residual principal stresses.
$\varepsilon_1, \varepsilon_2, \varepsilon_3$	Relaxed strains along the grid directions.
$\varepsilon_x, \varepsilon_y$	Relaxed strains along the principal residual stress directions.
$a, b$	Elastic calibration coefficients.
$e_v$	Error defined to validate the model.
$E, \nu$	Material elastic constants: Young's modulus and Poisson's ratio.
$\sigma_Y$	Material (initial) yield stress.
$E_T$	Tangent modulus in the elastic–plastic regime.
$R = E_T/E$	Strain hardening ratio.
$\Omega = \sigma_y/\sigma_x$	Residual stress biaxiality ratio.
$d_p$	Path dependency.
$\varepsilon_1^{pl}$	First principal plastic strain.
$\sigma_{eq}$	Equivalent residual stress (von Mises).
$\sigma_{eq,i}$	Equivalent residual stress at the onset of yielding.
$f$	Plasticity factor.
$\sigma_{x,el}, \sigma_{y,el}$	Residual principal stresses, considering the material as elastic.
$\sigma_{eq,el}$	Equivalent residual stress, considering the material as elastic.
$\Omega_{el}$	Stress biaxiality ratio, considering the material as elastic.
$f_{el}$	Plasticity factor, calculated from the elastically calculated residual stresses.
$W, \mu$	Parameters of the approximation fit function $f - f_{el}$ .
$w_i, m_i$	Approximation fit coefficients to find the parameters $W, m$ , respectively.
$\hat{f}$	Procedure estimated plasticity factor.
$\hat{\sigma}_{eq}$	Procedure estimated equivalent residual stress.
$\hat{\sigma}_x, \hat{\sigma}_y$	Estimated principal residual stress components.
$Z_1, Z_2, Z_3, Z_4$	Hole depths used in the application example.
$\varepsilon'_0, \varepsilon'_1, \varepsilon'_2, \dots$	Relaxed strain function harmonic intensities (even order terms only).

## 1 Introduction

Blind hole drilling is a widely applied method for measuring residual stresses in materials that can be easily machined, such as metals. The relaxed strain field locally produced in a prestressed component by the introduction of the hole is generally measured by a rosette, typically carrying three strain gages with radially oriented grids [1]. Recently, other methods have been proposed to measure the relaxed strain field, such as the Laser Speckle Interferometry [2] and the Moiré Interferometry [3]. These optical techniques provide a “full field” detection of the relaxed displacement field near the hole, while the rosette only gives the strains in radial directions averaged on the areas of three grids. Though the optical methods can be also used to determine a non-uniform residual stress profile [4, 5], the method based on the strain gage rosette is simpler, more physically robust, and better suited to field use.

In general, the residual stress evaluated by the strain gage hole drilling method is affected by several errors or sources of inaccuracy, some of which have to be limited by increasing the quality of the procedures while

others can be corrected by a proper elaboration of the results [6]. The present paper is focused on correcting the effect of the local plasticity which is produced when measuring high residual stresses in ductile materials. If the level of the residual stress is comparable with the material yield stress, the stress concentration due to the hole produces zones in which the elastic limit of the material is reached. The plastic region arises at the lower circumference of the hole (the edge at the flat bottom surface) then it spreads toward the strain gages when the hole depth is increased [7, 8]. This phenomenon is significant when evaluating the most intense and, for this reason, the most interesting residual stress fields such as those generated by shot peening [9, 10], welding [11, 12] or friction stir welding [13] particularly nearby the welding zone. As the plasticity makes the material more compliant, if the measured relaxed strains are elaborated by means of the usual procedures based on the assumption that the material is linear elastic, the obtained residual stress is overestimated.

The Kirsch classic solution [14] of the equivalent ideal two-dimensional problem represented by a plane membrane in which a passing-through hole is performed, can be used to estimate the maximum residual stress under which the material remains elastic. It can be noted that the maximum residual stress for the elastic behavior of the material depends on the residual stress biaxiality ratio. For instance, under uniaxial residual stress ( $\sigma_x = \sigma_0$  and  $\sigma_y = \tau_{xy} = 0$ ) the plasticity onset happens for  $\sigma_0 = \sigma_Y/3$  (where  $\sigma_Y$  is the material yield stress), under equibiaxial residual stress ( $\sigma_x = \sigma_y = \sigma_0$  and  $\tau_{xy} = 0$ ) at  $\sigma_0 = \sigma_Y/2$  and under pure shear ( $\sigma_x = -\sigma_y = \sigma_0$  and  $\tau_{xy} = 0$ ) at  $\sigma_0 = \sigma_Y/4$ . Even though the Kirsch solution is valid only in the plane problem, a finite element analysis shows that similar elastic limits can be assumed for a *deep* blind hole performed on a *thick* plate, under uniform through-thickness biaxial residual stress. According to the ASTM E 837–08 standard, a deep hole has to have a minimum depth of 0.4 the rosette mean diameter  $D$ , and the plate is considered thick if its thickness is at least  $1.2D$  [1].

Nevertheless, an ideal blind hole shows a sharp notch at the lower circumference of the hole and in an elastic analysis a stress singularity is expected. Consequently, plasticity occurs at the lower circumference of the hole for any hole depth with any non zero residual stress and, to be precise, the linearity between the strain gage response and the residual stress is lost even for very low residual stress and any biaxiality ratio. However, accurate elastic–plastic numerical solutions demonstrate that the strain reading is affected by the plasticity only when a significant volume of the region surrounding the hole is in the plastic regime. Moreover, considering the practical application of the testing procedure, the maximum stress that can be accurately evaluated by means of the elastic elaboration of the blind hole drilling method is even larger than that predicted by the plane Kirsch solution. Indeed, the ASTM E837–08 standard suggests that the elastic elaboration of the relaxed strain can be accepted up to a maximum residual stress of  $0.6\sigma_Y$ , after the cited study of Beghini et al. on the effect of plasticity Reference [15].

However, if the residual stress measured by the ASTM E837–08 standard is higher than  $0.6\sigma_Y$ , the obtained value has to be considered overestimated and the measurement rejected. In the present paper, a correction procedure by which the ASTM E837–08 standard can be extended up to  $\sigma_Y$ , taking into account of the plasticity, is proposed. The present work is an extension and an improvement of the preliminary proposal of Beghini et al. [16, 17]. A more accurate finite element elastic–plastic parametric analysis has been developed and a more accurate, and general, correcting procedure is provided which can be applied to all the rosettes available on the market. Moreover, the previous research was limited to the deep hole configuration, while in the present study four hole depth configurations were investigated. This can be considered a first step in the solution of the complex and yet not solved problem of the measurement of high and variable though the thickness residual stress. Indeed, one of the main limitations of any plasticity correction procedure is due to the fact that the superimposition principle is not applicable. As a consequence, a uniform through thickness residual stress distribution has to be assumed across the entire hole depth, as depicted in Figure 1, and then the information gained by measuring the relaxed strains at incremental depths cannot be directly considered. In the present paper, this limitation is partially overcome by proposing a correction procedure for each of four hole depth configurations. If the residual stress is not expected to have a uniform distribution, approximate averaged residual stress levels can be deduced at the different depths (the uniform stress is acceptable at least in the first step which is very shallow). By comparing the different residual stresses calculated as uniform for the partial hole depths, an indication of the trend is obtained.

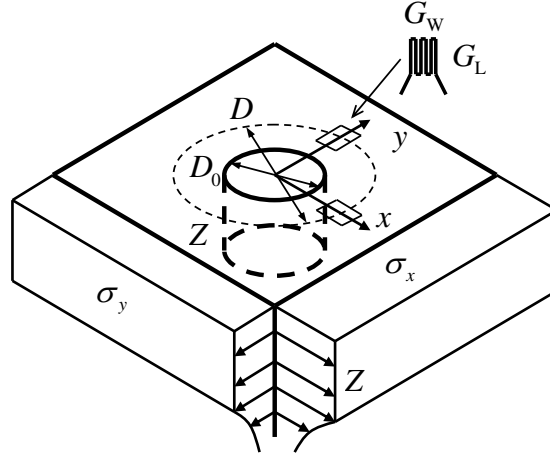


Figure 1: Blind hole drilling scheme, principal residual stresses are assumed uniform across the hole depth (adapted from ASTM E837–08 [1]).

The method described in the paper, to take into account for the hole drilling plasticity effect, requires the advance knowledge of the principal stress directions, because the strain gage rosette, Figure 1, must be attached to the test specimen such that the two orthogonal grids are aligned with the principal stresses, and only the two orthogonal grids relaxed strain readings are used. If the rosette is not aligned with the principal directions and plastic deformations are significant, the three grids strain gage rosette, typically used for hole drilling measurements, do not provide sufficient information. The use of a four grids strain gage rosette has been suggested in Reference [17] to evaluate the principal directions misalignment angle and reproduce the as principally aligned relaxed strain, to be then used as input for the procedure.

## 2 Strain gage rosettes

All the rosettes available on the market for residual stress evaluation have been considered in the present analysis, Table 1. As the grid dimensions are not very different, the corresponding calibration coefficients are quite similar. However, in this kind of measurement and elaboration any source of errors has to be reduced as much as possible because also apparently small differences can produce not negligible biases. The rosettes HBM RY61K and HBM RY61S have different grid layout but same grid dimensions:  $D$ ,  $G_L$ ,  $G_W$ , so they have the same response to plasticity. The Vishay 062RE type actually is a group of three self-similar rosettes with gage circle diameters:  $D = 2.57, 5.13, 10.26$  mm and proportional grid length and width  $G_L$ ,  $G_W$ . Also for them, the plasticity effect is the same because of the similarity of geometry.

Name used in the paper	Datasheet name	$D$ [ mm ]	$G_L$ [ mm ]	$G_W$ [ mm ]	Reference
ASTM A	Vishay 062RE	5.13	1.59	1.59	[1, 18]
ASTM B	Vishay 062UM	5.13	1.59	1.14	[1, 18]
HBM 1	HBM RY21	10.2	3.0	2.5	[19]
HBM 2	HBM RY61K(S)	5.10	1.50	0.70	[19]
HBM 3	HBM RY61R	5.10	1.50	0.72	[19]

Table 1: Strain gage rosettes and grid dimensions.

The ASTM E837–08 standard indicates the type A rosettes with the grids spaced according to the  $0^\circ/90^\circ/135^\circ$  pattern, while the type B with the grids at  $0^\circ/45^\circ/90^\circ$ . The angular difference is important when the principal direction of the residual stress field has to be obtained and when the eccentricity is considered [20]. In the

present study, the different sequence of grid angles does not play any role. However, the distinction between type A and type B is relevant due to the different width of the grid.

The calibration coefficients  $a$  and  $b$  are defined in the ASTM E 837–08 standard [1] for a uniform trough–thickness residual stress up to the maximum hole depth, and assuming the material linear elastic. Indicating with  $x, y$  the principal directions of the residual stress field and assuming that two grids are oriented in those directions, Figure 1, the principal residual stresses  $\sigma_x, \sigma_y$  and the measured relaxed strain  $\varepsilon_x, \varepsilon_y$  are related by the following relationships:

$$\sigma_x = -\frac{E(\varepsilon_x + \varepsilon_y)}{2a(1 + \nu)} - \frac{E(\varepsilon_x - \varepsilon_y)}{2b}, \quad \sigma_y = -\frac{E(\varepsilon_x + \varepsilon_y)}{2a(1 + \nu)} + \frac{E(\varepsilon_x - \varepsilon_y)}{2b} \quad (1)$$

where:  $E, \nu$  are the material Young’s modulus and the Poisson’s ratio respectively. The calibration coefficients  $a$  and  $b$  depends on geometric quantities and the material elastic properties, and they can be obtained with a calibration procedure based on a direct measurement of a known stress field or, more conveniently, through a finite element simulation of residual stress measurement. By applying a known residual stress field with  $\sigma_x \neq \sigma_y$ , after measuring or numerically evaluating the relaxed strain  $\varepsilon_x, \varepsilon_y$  produced by drilling the hole, Equations 1 can be used to deduce the calibration coefficients  $a$  and  $b$ . The calibration coefficients are reported in Appendix A, Table 3, for  $\nu = 0.3$  for all the considered rosettes and the several ratios:  $Z/D, D_0/D$  where  $Z$  is the hole depth and  $D_0$  is the hole diameter. The accurate finite element model used to find the calibration coefficients is explained in the following section. This model was used to perform the elastic–plastic analyses too, by introducing the specific elastic–plastic constitutive material model.

### 3 Finite element model

#### 3.1 General features

A Finite Element (FE) model was set up to numerically evaluate the relaxed strain readings for different geometric configurations and material properties. The assumptions of the analysis and the model features are summarized in the following:

- owing to symmetries, the finite element model was reduced to 1/4 of the entire volume, Figure 2;
- the model width was chosen 30 times the hole diameter  $D_0$  and the thickness 1.2 times the rosette mean diameter  $D$ , according to the minimum thickness recommended by the ASTM E 837–08 standard for thick plates, Figure 2;
- bilinear stress–strain curve and isotropic strain hardening plasticity model were assumed, thus material is completely defined by the elastic properties  $E, \nu$ , the yield stress  $\sigma_Y$  and the strain hardening ratio  $R = E_T/E$ , Figure 3.

#### 3.2 FE model validation

The distributions of the elements on the plane and along the depth were preliminary examined in order to obtain an accurate numerical reproduction of the phenomenon. In this phase a linear elastic material was considered as reference. A plane stress finite element model with the same element distribution was assessed by comparison with the Kirsch plane stress solution (provided by Schajer [21]).

The relaxed strains obtained by the plane model showed differences  $e_v < 1\%$  as compared to the analytical solution so the in–plane element distribution was considered accurate enough.

A similar assessment of the through the thickness nodal distributions was not possible as an equivalent analytical reference solution is not available for the blind hole, even in the elastic regime. For this reason, a very refined model made by plane *harmonic* elements was set up to produce accurate reference solutions in the

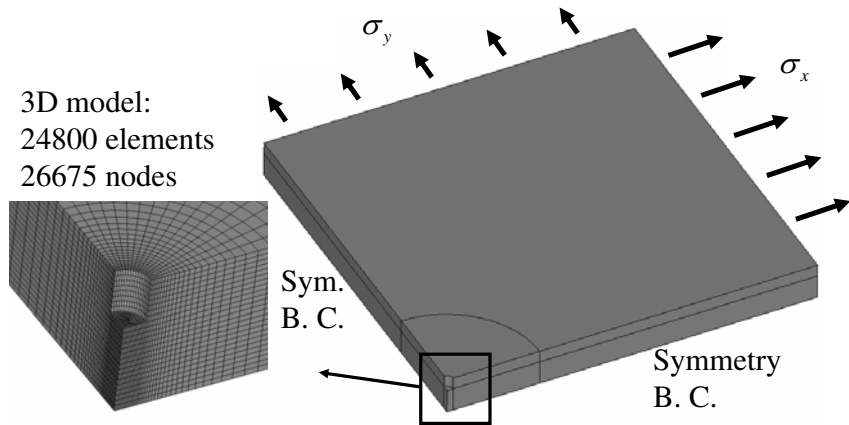


Figure 2: Solid tridimensional FE model.

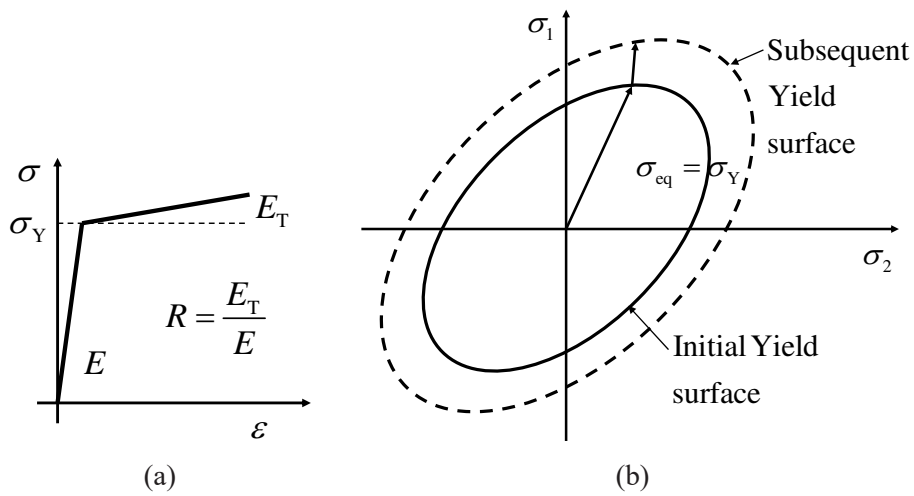


Figure 3: Assumed material constitutive law: bilinear isotropic hardening.

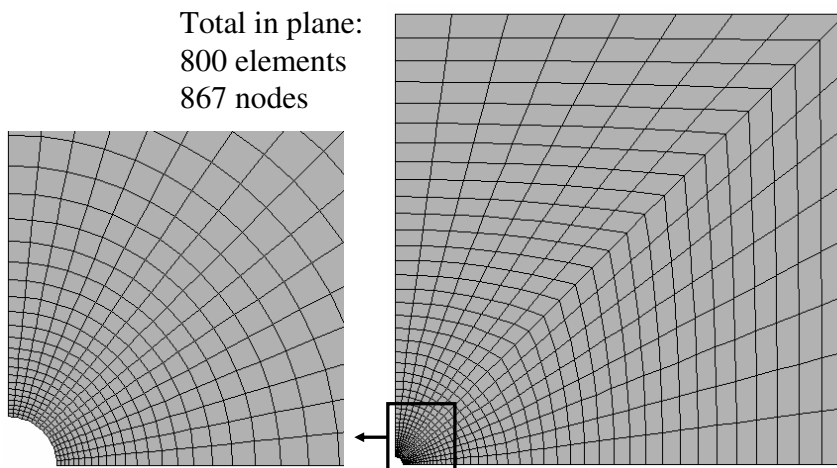


Figure 4: Surface element distribution producing a percentage error below 1%.

elastic regime. Again, the relative differences with the three-dimensional model was below 1%. Therefore, also the discretization along the depth of the three-dimensional model was assumed accurate enough. The



validated three-dimensional FE model, used for all the elastic-plastic analyses reported in the following, is shown in Figure 2.

### 3.3 Loading sequence

If the finite element analyses is intended to accurately reproduce the plasticity generated during the hole drilling, the actual evolution of the hole on a body affected by the residual stresses should be modeled. This can be properly obtained either by using the “birth and death” elements or by drastically reducing the Young’s modulus of the elements at the layers to be removed. These two equivalent procedures are here called the “hole-after-residual stress” approach. If the material were linear elastic, or hyperelastic at least, the relaxed strain measured by the rosette could be alternatively obtained by the “loading-after-hole” approach, i.e. by simulating the application of the stress on a plate already carrying the hole, since the solution is not path dependent (provided that the strain at the gage location calculated with no hole is subtracted).

The “loading-after-hole” approach is the typical FE procedure used for determining the elastic calibration coefficients as it is simpler to be applied and computationally more efficient. Unfortunately, in the presence of plasticity, the final stress/strain distribution depends on the loading sequence (path dependent solution) and the “hole-after-residual stress” approach should be applied. However, when plasticity occurs, the “loading-after-hole” approach is even more computationally efficient than the “hole-after-residual stress” approach as a single load step is imposed in the former case while multiple load steps are to be applied in the latter case. For this reason, a case study was performed and a comparison between the predictions of the two approaches was obtained for the elastic-plastic phenomenon under consideration. The results of an ASTM A rosette and typical hole diameter  $D_0/D = 0.4$  are presented by comparing the loading-after-hole FE model and the hole-after-residual stress approaches applied to the same finite element model under the same stress. Similar results were found for other rosettes and test parameters.

In general, the two approaches were found to produce negligible differences in terms of the relaxed strain. The relative differences were found in the order of a few percent, even in the worst condition of an almost perfectly plastic material, and dependent on the biaxiality ratio:  $\Omega = \sigma_x/\sigma_y$ . The maximum difference  $d_p$  was found for  $\Omega = 0.668$ , Figure 5.

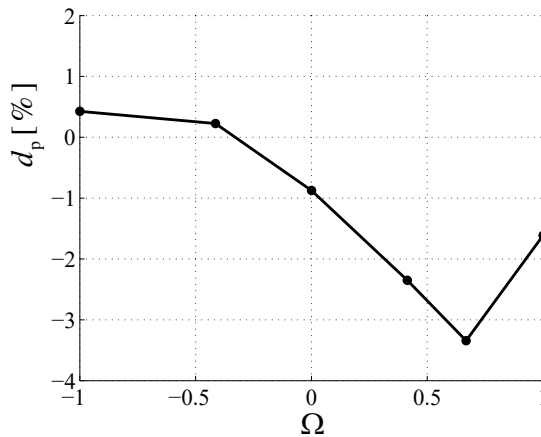


Figure 5: Loading-after-hole to hole-after-residual stress approaches path dependency relative difference.

The maps of the first principal plastic strain  $\epsilon_1^{pl}$ , obtained by following the two approaches, for the worst condition  $\Omega = 0.668$ , are shown in Figure 6.

When applying the “loading-after-hole”, the region that experiences plasticity is a slightly larger, however the error due to the path dependence  $d_p$  is very small because the strain gage grids that measure the relaxed strain are at a certain distance from the plastic region. The condition shown in the figure refers to a rather high plastic effect and the path dependence reduces quickly for a lower residual stress.



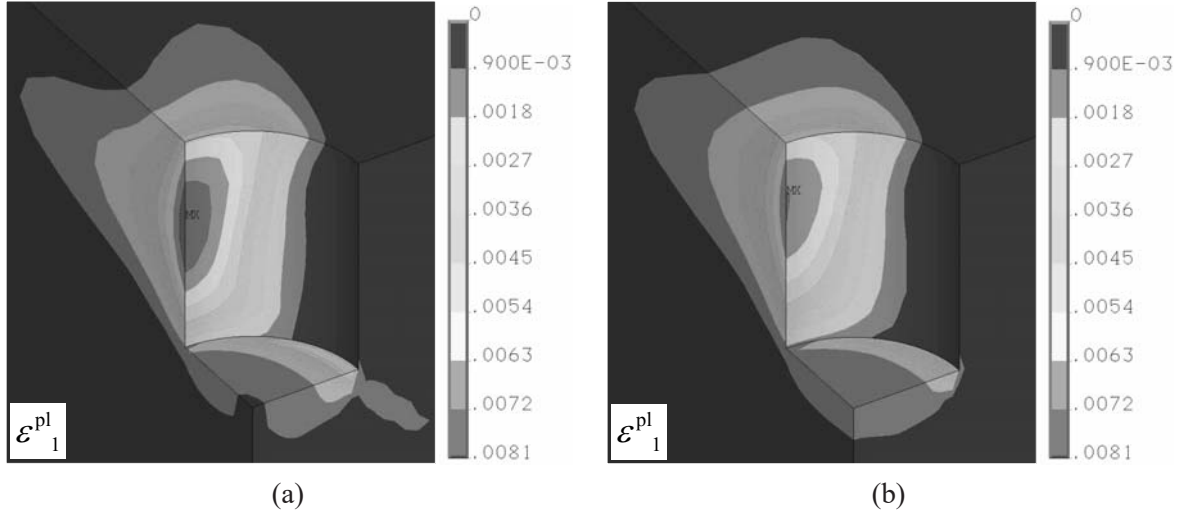


Figure 6: First principal plastic strain,  $\Omega = 0.668$ , imposed residual stress very near the material yield stress: (a) “loading–after–hole” approach; (b) “hole–after–residual stress” approach.

The present results do not confirm the data published in the paper by Moharami and Sattari–Far [12] who indicated a strong path dependence at the same loading conditions reported here. However, in the authors’ opinion, the present results appear more justifiable. Indeed, the plastic zone which can be produced in the hole drilling is dominated by the prevailing surrounding elastic region and it can be verified that the most points of the model experience an increasing stress history even when the “hole–after–residual stress” approach is applied. It is worth noting that the negligible effect of the loading sequence gives also the possibility to design experimental verifications of the elastic–plastic analysis by controlling the remote load on a specimen. The same tests would be much more difficult to be obtained using several specimens affected by different and controlled residual stresses [12].

After having verified a general negligible effect due to the load sequence, the FE database developed in order to elaborate the correction procedure was obtained following the more efficient “loading–after–hole” approach: the simulation time following this approach was approximately 5 minutes on a modern PC desktop while with the other approach the simulation time was 10 times higher.

### 3.4 Plasticity factor

The Von Mises equivalent stresses  $\sigma_{eq} = \sqrt{\sigma_x^2 + \sigma_y^2 - \sigma_x \sigma_y}$  was assumed for quantify the effect of biaxiality and, in accordance with Reference [17], a dimensionless plasticity factor was introduced:

$$f = \frac{\sigma_{eq} - \sigma_{eq,i}}{\sigma_Y - \sigma_{eq,i}} \quad (2)$$

where:  $\sigma_{eq,i}$  is the equivalent residual stress producing the onset of plasticity in the two dimensional case and  $\sigma_Y$  the material yield stress. The plasticity factor measures the residual stress intensity with respect to the approximate onset of plasticity given by the plane Kirsch solution. The equivalent residual stress at the plasticity onset can be expressed as a function of the the biaxiality ratio  $\Omega = \sigma_y/\sigma_x$ , according to the plane stress Kirsch solution:

$$\sigma_{eq,i} = \sigma_Y \frac{\sqrt{1 - \Omega + \Omega^2}}{3 - \Omega} \quad (3)$$

Following the Equations 2,3,  $f = 0$  represents the condition of the highest residual stress that still does not produce plasticity while  $f = 1$  is related to the residual stress producing general yielding in the whole body.

As previously observed, also small positive plasticity factor (e.g.  $f = 0.01$ ) does not produce significant plasticity effect on the measurement, because the  $\sigma_{eq,i}$  is defined according to the Kirsch plane stress model and the limited plastic region at the lower circumference of the hole, which is produced also for  $f < 0$ , does not significantly affect the relaxed strain on the surface as compared to the elastic field.

### 3.5 Investigated configurations

Any measurement configuration is defined by: rosette type, i.e. the dimensionless ratios  $G_L/D, G_W/D$ , hole diameter  $D_0/D$  and depth  $Z/D$ , biaxiality ratio  $\Omega = \sigma_x/\sigma_y$ , and material strain hardening ratio  $R = E_T/E$ . For any configuration the readings of the rosette were obtained as a function of the residual stress level  $f$ . A database of finite element simulations was produced by performing an extensive parametric analysis which is summarized in the following:

- rosette types with the dimensions reported in Table 1;
- hole diameter  $D_0/D = 0.3, 0.35, 0.4, 0.45, 0.5$ ;
- strain hardening ratios  $R = 0.01, 0.1, 0.25$ ;
- biaxiality ratios  $\Omega = -1.000, -0.414, 0.000, 0.414, 0.668, 1.000$ ;
- plasticity factors  $f = 0.0, 0.1, 0.2, 0.3, 0.4, 0.5, 0.6, 0.7, 0.8, 0.9, 0.99$ ;
- hole depths  $Z/D = 0.02, 0.1, 0.2, 0.4$ .

The combinations of plasticity factors and biaxiality ratios are shown in Figure 7.

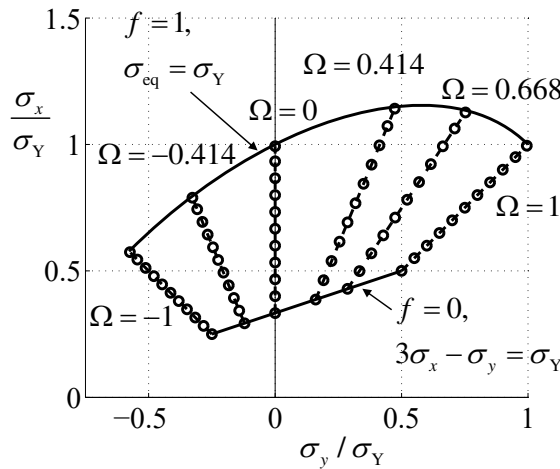


Figure 7: Combinations of plasticity factors and biaxiality ratios.

In order to take advantage of the symmetry of material properties, the condition  $|\sigma_x| > |\sigma_y|$  was assumed thus limiting the region of the Haigh–Westergaard plane  $\sigma_x - \sigma_y$  to the portion reported in Figure 7 ( $|\Omega| \leq 1$ ) without reducing the generality of the results. This implies that the direction of the maximum absolute value of the measured relaxed strain has to be the  $x$  axis.

The total number of three–dimensional elastic–plastic analyses was:  $5 \times 5 \times 3 \times 6 \times 11 \times 4 = 19800$ . A powered PC desktop takes approximately 5 minutes for each simulation at 100% time of elaboration, so approximately 1 700 hours (= 70 full days) were required to complete the database.

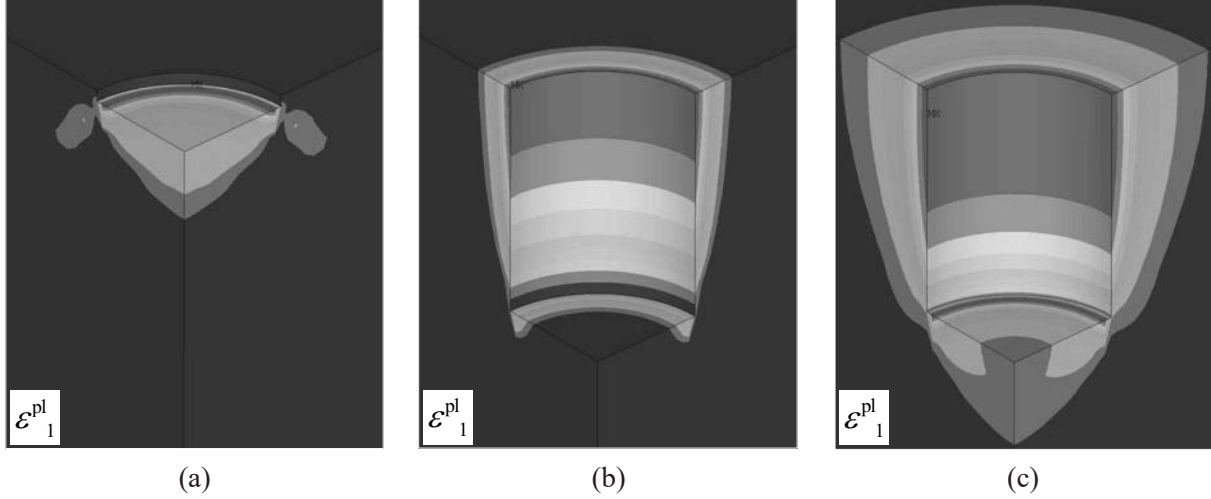


Figure 8: First principal plastic strain distribution: (a) shallow hole, plasticity factor  $f = 0.99$ , maximum first principal plastic deformation  $\varepsilon_1^{\text{pl}} = 0.623 \times 10^{-3}$ ; (b) deep hole, plasticity factor  $f = 0.5$ , max.  $\varepsilon_1^{\text{pl}} = 1.26 \times 10^{-3}$ ; (c) deep hole, plasticity factor  $f = 0.99$ , max.  $\varepsilon_1^{\text{pl}} = 3.20 \times 10^{-3}$ .

### 3.6 Results

Typical results of the shallow hole and the deep hole configurations for  $\Omega = 1$ , rosette type ASTM A, diameters ratio  $D_0/D = 0.4$ , strain hardening ratio  $R = 0.01$  are reported in Figure 8.

It can be observed that for the shallow hole the plastic region is located below the hole bottom surface. The plastic region reaches the surface for the deep hole, and for values of  $f$  approaching unity, particularly for materials with low strain hardening, the surface plastic boundary intersect the grid region.

After imposing the loading conditions and having obtained the solution, the simulated strain of the rosette  $\varepsilon_x, \varepsilon_y$  were calculated from the displacements difference, along the grid direction, at the two ends of the grid divided by the grid length. The FE simulated strain was then processed by means of the elastic calibration coefficients  $a$  and  $b$ , Table 3 in order to obtain the “as elastically evaluated” residual stresses, i.e. the stress components that would result from the measured strain, by assuming the material as linear elastic [17].

$$\sigma_{x,\text{el}} = -\frac{E(\varepsilon_x + \varepsilon_y)}{2a(1+\nu)} - \frac{E(\varepsilon_x - \varepsilon_y)}{2b}, \quad \sigma_{y,\text{el}} = -\frac{E(\varepsilon_x + \varepsilon_y)}{2a(1+\nu)} + \frac{E(\varepsilon_x - \varepsilon_y)}{2b} \quad (4)$$

The elastically evaluated equivalent stress can be defined as:

$$\sigma_{\text{eq,el}} = \sqrt{\sigma_{x,\text{el}}^2 + \sigma_{y,\text{el}}^2 - \sigma_{x,\text{el}}\sigma_{y,\text{el}}} \quad (5)$$

and the related elastically evaluated plasticity factor is obtained by the equation:

$$f_{\text{el}} = \frac{\sigma_{\text{eq,el}} - \sigma_{\text{eq,i}}}{\sigma_Y - \sigma_{\text{eq,i}}} \quad (6)$$

So far, the ASTM interpretation procedure has been applied ignoring the effect of plasticity. Consequently, if a significant plasticity is produced, the elastically calculated plasticity factor is larger than the actual plasticity factor. As the plasticity is not expected to play a significant role for plasticity factor near 0, it follows that  $f_{\text{el}} \approx f$ , when  $f \ll 1$ . The following function:

$$f_{\text{el}} = f + Wf^\mu \quad (7)$$

was found to accurately fit the relationship between  $f$  and  $f_{\text{el}}$  for any considered configuration. The expression is a novelty as compared to the proposal of the Reference [17] in which a simpler quadratic function was

used. The main reason for adopting this more general expression (Equation 7 becomes a quadratic expression when  $\mu = 2$ ) is mainly due to the broader range of configurations considered in the present analysis, in particular the shallow hole required an exponent  $\mu$  significantly higher than 2. It can be observed that the asymptotic behavior of the function at low  $f$  values is fulfilled by the proposed expression for any values of the parameters  $W$  and  $\mu$ . The parameters  $W$  and  $\mu$  were found for any analyzed material and geometrical configuration by means of a least-square fitting which was found to produce excellent results. Comparisons between the FE solutions and the obtained fitting curves are shown in Figure 9 for the rosette type ASTM A, depth  $D_0/D = 0.4$  and considering the most challenging conditions for the strain hardening ratio  $R = 0.01$ .

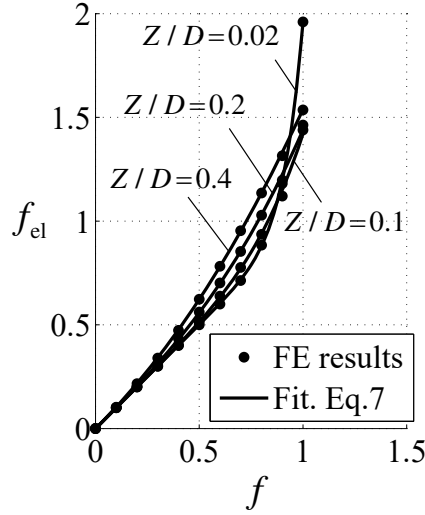


Figure 9: Relation between the imposed plasticity factor  $f$  and the elastically calculated plasticity factor  $f_{el}$ ,  $R = 0.01, D_0/D = 0.4$ , depth ratios:  $Z/D = 0.02, 0.1, 0.2, 0.4$ , rosette type ASTM A.

In general, the obtained parameters  $W, \mu$  depend on  $Z/D, D_0/D, \Omega, R$  and on the rosette geometry  $G_L/D, G_W/D$ . As a unique function representing  $W, \mu$  was considered too complicated to be obtained with the required level of accuracy, it was decided to obtain specific functions  $W, \mu$  of  $\delta = D_0/D$  and  $\Omega$  only for any rosette. Figure 10 shows the  $W(\delta, \Omega), \mu(\delta, \Omega)$  functions for the ASTM A rosette type, depth ratio  $Z/D = 0.4$ , and different strain hardening ratios. Other configurations showed similar trends.

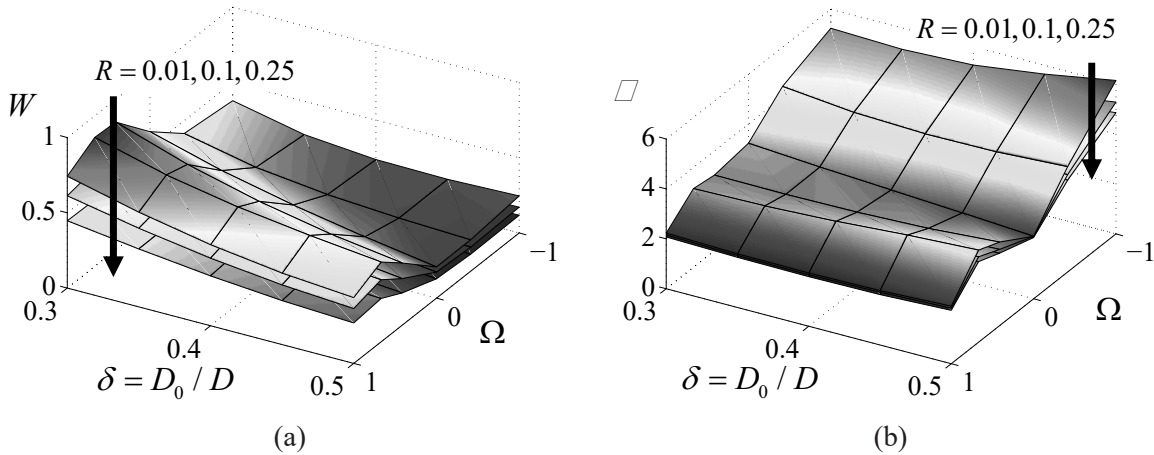


Figure 10: Rosette type ASTM A,  $Z/D = 0.4$ , different strain hardening ratios  $R = 0.01, 0.1, 0.25$ : (a)  $W(\delta, \Omega)$ , (b)  $m(\delta, \Omega)$ .

Bivariate polynomials were introduced for expressing the parameters  $W, m$  as functions of the dimensionless

ratios  $\delta$  and  $\Omega$ . It is worth noting that both coefficient functions show a parabolic trend with respect to  $\delta$  (no inversion of curvature) while they show an inversion of curvature with respect to  $\Omega$ , that can be approximated with a cubic relationship. So the polynomial functions to be introduced need to have the terms in  $\delta^2, \delta$ , the terms in  $\Omega^3, \Omega^2, \Omega$ , the combined terms and the degree zero term:

$$\begin{aligned}
 W &= w_1\Omega^3\delta^2 + w_2\Omega^2\delta^2 + w_3\Omega\delta^2 + w_4\delta^2 + w_5\Omega^3\delta + w_6\Omega^2\delta + w_7\Omega\delta + w_8\delta + \\
 &\quad w_9\Omega^3 + w_{10}\Omega^2 + w_{11}\Omega + w_{12} \\
 \mu &= m_1\Omega^3\delta^2 + m_2\Omega^2\delta^2 + m_3\Omega\delta^2 + m_4\delta^2 + m_5\Omega^3\delta + m_6\Omega^2\delta + m_7\Omega\delta + m_8\delta + \\
 &\quad m_9\Omega^3 + m_{10}\Omega^2 + m_{11}\Omega + m_{12}
 \end{aligned} \tag{8}$$

A further least-squares fitting was then performed to find the coefficients  $w_i, m_i (i = 1 \dots 12)$ . The final results are reported in Table 4 of Appendix A for all the rosettes, strain hardening ratios and hole depths.

### 3.7 Effect of stress biaxiality

The present finite element simulations confirmed the observation that the ratio between the measured relaxed strains along the principal directions  $\epsilon_x/\epsilon_y$  depends on the stress ratio  $\Omega$  but it is almost not affected by the plasticity factor, as shown in Figure 11. As a consequence, the biaxiality ratio  $\Omega$  can be approximated by the ratio between the elastically calculated residual stress components  $\sigma_{x,el}, \sigma_{y,el}$ :

$$\Omega = \frac{\sigma_y}{\sigma_x} \approx \Omega_{el} = \frac{\sigma_{y,el}}{\sigma_{x,el}} \tag{9}$$

As explained in the following, this approximate relationship is particularly useful to simplify the correction procedure.

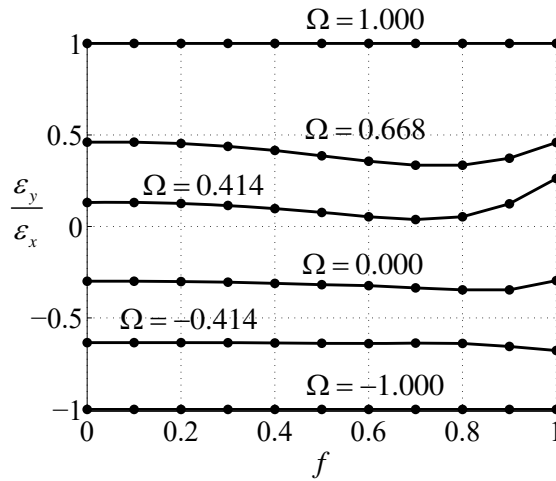


Figure 11: Weak dependence of the ratio between relaxed strain on the plasticity factor.

## 4 Correction procedure for the effect of plasticity

The elaboration of the finite element results explained in the previous sections gives the tools for developing a procedure to measure high residual stress which includes a correction of the elastically evaluated stress in order to account for the plasticity effect, if necessary. The procedure is summarized in the following steps:

1. the strain gage rosette is applied on the surface of the body affected by residual stress with the 1 and 3 grids aligned with the known (or at least assumed) principal residual stress directions and the signals are set to zero;

2. the relaxed strain  $\varepsilon_1, \varepsilon_2, \varepsilon_3$  are measured after the hole, the  $x$  axis is chosen parallel to the grid measuring the maximum absolute value, therefore if  $|\varepsilon_1| > |\varepsilon_3|$ , then  $\varepsilon_x = \varepsilon_1$  and  $\varepsilon_y = \varepsilon_3$ , otherwise  $\varepsilon_x = \varepsilon_3$  and  $\varepsilon_y = \varepsilon_1$ ;
3. the elastically evaluated residual stresses  $\sigma_{x,el}, \sigma_{y,el}$  are determined from the Equations 4;
4. the elastically calculated biaxiality ratio  $\Omega_{el}$  is assumed an accurate approximation of the actual residual stress biaxiality ratio  $\Omega$ , Equation 9;
5.  $f_{el}$  can be obtained from the Equation 6, with the equivalent residual stress at the yield onset  $\sigma_{eq,i}$  obtained from Equation 3;
6. if  $f_{el} < 0$  no correction is required, and the elastically evaluated residual stresses are assumed as the actual residual stresses, otherwise the plastic correction is required and the procedure continues in the following steps;
7. the coefficients  $w_i, m_i (i = 1 \dots 12)$  are obtained from Table 4 for the given rosette hole depth and material;
8. the coefficients  $W, \mu$  are obtained from Equations 8;
9. the actual  $f$  has to be obtained from  $f_{el}$  by inverting Equation 7, to solve this not elementary equation the Newton–Raphson algorithm is recommended which gives an accurate numerical approximation of the plasticity factor hereafter called  $\hat{f}$ , for details see Appendix B;
10. the estimated equivalent residual stress  $\hat{\sigma}_{eq}$  is obtained from the plasticity factor  $\hat{f}$ :

$$\hat{\sigma}_{eq} = \sigma_{eq,i} + \hat{f}(\sigma_Y - \sigma_{eq,i}) \quad (10)$$

11. finally, the estimated principal residual stress components  $\hat{\sigma}_x, \hat{\sigma}_y$  are obtained from  $\hat{\sigma}_{eq}$ :

$$\hat{\sigma}_x = \hat{\sigma}_{eq} \frac{1}{\sqrt{1 - \Omega + \Omega^2}}, \quad \hat{\sigma}_y = \Omega \hat{\sigma}_x \quad (11)$$

A numerical example of the practical application of the procedure is reported hereafter. As shown in Figure 12, the measurement of a through–thickness uniform uniaxial tensile residual stress was numerically simulated with the following parameters: material yield stress  $\sigma_Y = 500$  MPa, strain hardening ratio  $R = 0.01$ ,  $\sigma_x = 0.95\sigma_Y = 475$  MPa (not equivalent to  $f = 0.95$ ), ASTM A rosette with diameter  $D = 5.13$  mm and hole  $D_0 = 0.4D$ .

All the quantities obtained during application of the the procedure are reported in Table 2 for the four hole depths  $Z_1 = 0.02D, Z_2 = 0.1D, Z_3 = 0.2D, Z_4 = 0.4D$ .

The Table 2 also shows the relative error (percent) between the estimated residual stress assuming the material as elastic  $\sigma_{eq,el}$ , i.e. not taking into account the plasticity effect, and the (actual) equivalent stress  $\sigma_{eq}$ . It is worth noting that this error is in the range 15% – 18%, while the error of the correction procedure itself  $(\hat{\sigma}_x - \sigma_x)/\sigma_x$  is much lower (3% – 5%).

## 5 Discussion

Because of the introduced approximations (mainly due to the fitting functions and the assumed independence of the biaxiality ratio to the stress level) the procedure is not expected to exactly reproduce the imposed value even in a calibration experiment made by a numerical simulation. The “self consistency” of the model was therefore tested in order to estimate the capability of the procedure to reproduce residual stress imposed in a condition in which the other errors are not present. The numerically evaluated relaxed strain were then

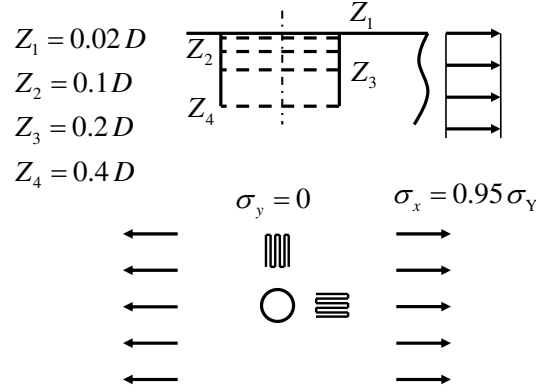


Figure 12: Monoaxial high residual stress to be reproduced by the BHD and the plasticity effect correction.

$Z_1 = 0.02D$	$Z_2 = 0.1D$	$Z_3 = 0.2D$	$Z_4 = 0.4D$
$\varepsilon_x = -65.4 \mu\epsilon$	$\varepsilon_x = -451.4 \mu\epsilon$	$\varepsilon_x = -774.4 \mu\epsilon$	$\varepsilon_x = -945.0 \mu\epsilon$
$\varepsilon_y = 12.8 \mu\epsilon$	$\varepsilon_y = 123.3 \mu\epsilon$	$\varepsilon_y = 229.9 \mu\epsilon$	$\varepsilon_y = 327.1 \mu\epsilon$
$\sigma_{x,el} = 553 \text{ MPa}$	$\sigma_{x,el} = 552 \text{ MPa}$	$\sigma_{x,el} = 537 \text{ MPa}$	$\sigma_{x,el} = 552 \text{ MPa}$
$\sigma_{y,el} = -20 \text{ MPa}$	$\sigma_{y,el} = -56 \text{ MPa}$	$\sigma_{y,el} = -41 \text{ MPa}$	$\sigma_{y,el} = -29 \text{ MPa}$
$f_{el} = 1.190$	$f_{el} = 1.248$	$f_{el} = 1.179$	$f_{el} = 1.202$
$\Omega_{el} = -0.036$	$\Omega_{el} = -0.102$	$\Omega_{el} = -0.077$	$\Omega_{el} = -0.052$
$\sigma_{eq,i} = 168 \text{ MPa}$	$\sigma_{eq,i} = 170 \text{ MPa}$	$\sigma_{eq,i} = 169 \text{ MPa}$	$\sigma_{eq,i} = 168 \text{ MPa}$
$W = 1.218, \mu = 16.0$	$W = 0.504, \mu = 6.36$	$W = 0.340, \mu = 4.47$	$W = 0.380, \mu = 3.34$
$\hat{f} = 0.912$	$\hat{f} = 0.930$	$\hat{f} = 0.932$	$\hat{f} = 0.917$
$\hat{\sigma}_x = 462 \text{ MPa}$	$\hat{\sigma}_x = 452 \text{ MPa}$	$\hat{\sigma}_x = 459 \text{ MPa}$	$\hat{\sigma}_x = 460 \text{ MPa}$
$\hat{\sigma}_y = -17 \text{ MPa}$	$\hat{\sigma}_y = -46 \text{ MPa}$	$\hat{\sigma}_y = -35 \text{ MPa}$	$\hat{\sigma}_y = -24 \text{ MPa}$
$(\hat{\sigma}_x - \sigma_x)/\sigma_x = -2.7\%$	$(\hat{\sigma}_x - \sigma_x)/\sigma_x = -4.8\%$	$(\hat{\sigma}_x - \sigma_x)/\sigma_x = -3.4\%$	$(\hat{\sigma}_x - \sigma_x)/\sigma_x = -3.1\%$
$(\sigma_{eq,el} - \sigma_{eq})/\sigma_{eq} = 16\%$	$(\sigma_{eq,el} - \sigma_{eq})/\sigma_{eq} = 18\%$	$(\sigma_{eq,el} - \sigma_{eq})/\sigma_{eq} = 15\%$	$(\sigma_{eq,el} - \sigma_{eq})/\sigma_{eq} = 17\%$

Table 2: Values obtained in the application examples ( $1\mu\epsilon = 10^{-6} \text{ mm/mm}$ ).

elaborated by the proposed correcting procedure and the obtained residual stresses compared to the applied values, Figure 13. It can be observed that the maximum error was  $\pm 4\%$  at the highest residual stress level ( $f = 0.99$ ) and low strain hardening coefficients ( $R = 0.01$ ) while the relative difference is typically within  $\pm 1\% - 2\%$ .

It is worth noting that during the real application of the procedure several significant measurement issues are important, such as: hole eccentricity, hole diameter uncertainty, material properties not accurately known, in particular the yield stress and the strain hardening near the yielding point. It is worth noting that some of these important sources of errors affect the residual stress evaluation in the elastic regime as well. as a consequence, the estimated plasticity factor  $\hat{f}$  can differ to the actual plasticity factor  $f$  not only for the numerical approximations but, more likely, for these other sources or error. Considering this fact, the errors introduced by the not exact self consistency of the proposed correcting procedure can be considered negligible.

A limit of the procedure is that the residual stress has to be uniform over the entire hole depth, so variable through-thickness residual stress can not be completely deduced. The plasticity correction procedure is recommended if the residual stress is near the material yield stress, especially when elaborating a shallow hole, otherwise  $f$  and  $f_{el}$  are close and the correction is small. As a general indication, considering the model self consistency, and the need of the uniform stress assumption, the use of the correcting procedure is effective when the correction is higher than  $3\% - 5\%$  of the material yield stress. The Figure 14(a), equibiaxial stress state  $\Omega = 1$ , shows that the difference between the elastically evaluated equivalent residual stress and the



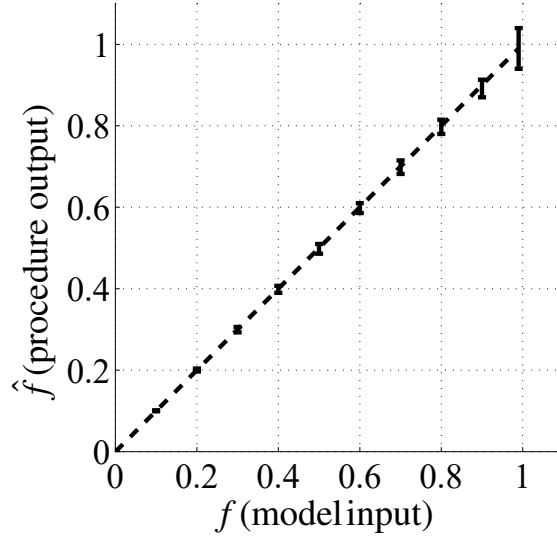


Figure 13: Model self consistency for all the 14 850 analyzed configurations.

actual equivalent residual stress is larger than 5% of the yield stress when the residual stress is higher than 70% of the yield stress for the deep hole configuration, and higher than 80–90% of the yield stress for the shallower hole configurations. These boundaries are even higher for lower biaxiality stress ratio, Figure 14(b). This important effectiveness boundary (and its dependencies with the depth and stress biaxiality ratio) can be considered an update of the conservative 60% that is reported, at the present, in the ASTM E837–08 standard [1].

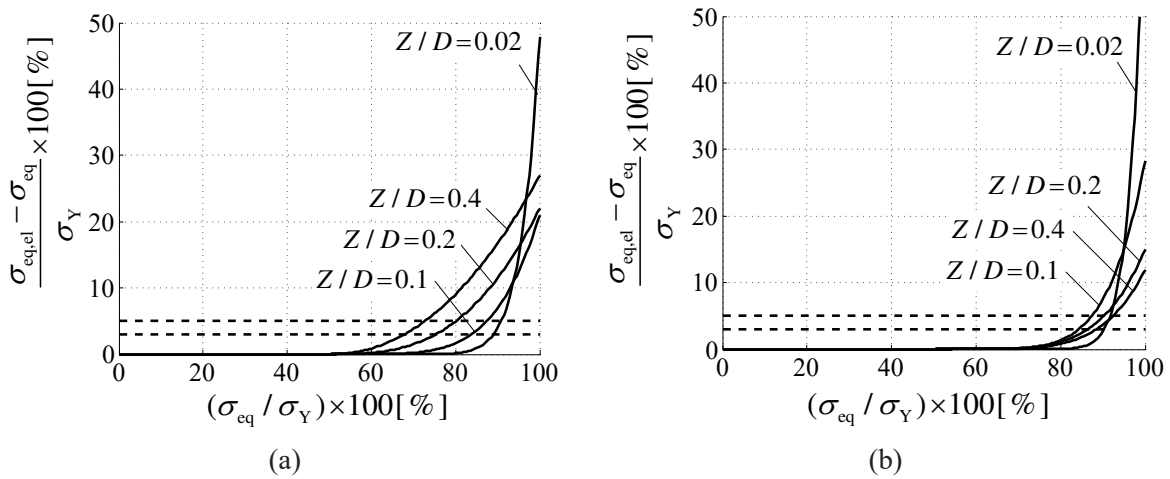


Figure 14: Proposed procedure effectiveness: (a) equibiaxial residual stress state  $\Omega = 1$ , (b) pure shear residual stress state  $\Omega = -1$ .

The proposed procedure can be applied if the principal residual stress directions are known and the strain gage rosette is aligned with the principal directions. In the elastic case, the orientation of the rosette does not affect the measurement, as the measured relaxed strain of a strain gage has the typical tensorial dependency on the orientation angle. The relaxed strain, as a function of the orientation angle, only contains a constant and a second order harmonic term:  $\varepsilon(\theta) = \varepsilon'_0 + \varepsilon'_1 \cos(2(\theta + \phi))$ . As a consequence, in the elastic regime, the entire function can be completely deduced by means of measurements at three angles to find the relaxed strain in the principal directions. Unfortunately, when the plasticity effect plays a role, the total (elastic plus plastic) strain becomes a more complex function of the grid direction angle. This function can be expressed by a typical

Fourier expansion including a constant term  $\varepsilon'_0$  and a series of harmonics of the type  $\varepsilon'_n \cos(2n(\theta + \phi))$  with ( $n = 1, 2, 3, \dots$ ). It can be observed that the intensities of higher terms vanish and the following expression is accurate enough:  $\varepsilon(\theta) \approx \varepsilon'_0 + \varepsilon'_1 \cos(2(\theta + \phi)) + \varepsilon'_2 \cos(4(\theta + \phi))$ , at least for  $f \leq 0.9$ , while for higher  $f$  also the terms  $\varepsilon'_3, \varepsilon'_4, \varepsilon'_5$  can be significant. Assuming that  $f \leq 0.9$  and unknown principal directions, the number of independent measured strains required is four, being four the unknowns:  $\varepsilon'_0, \varepsilon'_1, \varepsilon'_2, \phi$ . A rosette carrying four grids with specific angles is required [17], or even better a rosette with more than four grids. The relaxed strain along the principal direction can be then easily evaluated  $\varepsilon_{x(y)} = \varepsilon'_0 \pm \varepsilon'_1 + \varepsilon'_2$  ( $\varepsilon_x$  has to be the higher in absolute value). However, in several situations the directions of the principal residual stresses can be deduced by the symmetry of the geometry or by the process which induced the residual stress. For instance, the residual stress produced by shot peening has to be equibiaxial and every direction is principal so there is no possibility of misaligning the rosette gage grids (in this case only one grid would be required). An other example is rolling metalworking, the rolling direction and the orthogonal direction are obviously principal for the residual stress state.

Potentially, the optical methods are more suitable than the rosette method to determine the residual stress in the case of significant plasticity effect, because the whole strain field could be completely deduced, so the residual stress principal direction would follow.

The proposed procedure requires also that the material yield stress  $\sigma_Y$  is known. It is worth noting that many mechanical processes produce large local plastic strains, such as the shot peening surface treatment, and then they induce material work hardening which increases the local yield stress, so the knowledge of the effective yield stress could be not very accurate.

The hole geometry does not allow very large plastic strain. Only the first part of the stress–strain curve beyond the yield point is significant in this analysis. For some materials, in this part of the curve the bilinear model could be not very simple to be adapted as the curve slope can be continuously changing. The strain hardening ratio should be found by averaging the stress–strain curve up to the maximum strain that the material experiences during the hole drilling and a high  $R$ -ratio could be a better choice as compared to a low  $R$ -ratio that could be deduced by the whole stress–strain curve of the material. However, this uncertainty is not critical, since the correction function parameters are not very sensitive to the strain hardening ratio  $R$ , see Figure 10(a),(b), so a more complicated material model, that requires many parameters, is not recommended. The correction procedure defined for multiple depths partially faces the complex problem of analyzing the high residual stress with gradient along the depth. A preliminary residual stress evaluation can be produced by adopting the elastic hypotheses in order to find an approximated residual stress distribution. After this, it is common to find the highest level near the surface. In these condition, the plastic correction might be limited to the smallest depth, while the final part of the residual stress distribution could be approximated as the elastic solution preliminary found. Otherwise, the correction procedure could be applied for any of the hole depths assuming uniform stress, so deducing approximate information about the depth residual stress distribution. However, for a residual stress evaluation, aimed for instance at a fatigue strength assessment, only the residual stress near the surface is of interest, so the procedure can be conveniently used even though the residual stress is not uniform.

## 6 Conclusions

A procedure to correct the measurement of high residual stresses, with the blind hole drilling method, has been proposed by taking into account the plasticity effect. All the typical parameters were considered: the rosette type and dimensions, the hole diameter and depth, the material properties and the stress biaxiality ratios. By means of an extensive finite element analyses, an accurate database was obtained in which the effective residual stress loading was related to residual stress deduced by interpreting the relaxed strain assuming the material as elastic. The proposed correcting procedure derived from a proper elaboration of the finite element solutions database. The main results are summarized in the following.

- The “loading–after–hole” approach, instead of the correct but more time consuming “hole–after–residual

stress” approach, introduces a difference not exceeding 3% of the predicted residual stress, so this can be neglected since similar errors are also due to the material yield stress uncertainty, errors in the measurement, procedure fit function approximations and the uniform stress assumption.

- The analysis shows that, for deep holes ( $Z/D = 0.4$ ), the error of the elastic solution is less than 3% – 5%, for residual stresses up to 70% of the material yield stress, and a similar error bound is achieved for residual stresses up to 80% – 90% of the material yield stress, for shallower holes ( $Z/D \leq 0.2$ ). The stress correction procedure described here is useful to reduce stress evaluation errors in cases where the residual stresses are larger than these limits.
- When residual stresses close to the yield stress are to be measured a shallow hole is preferred, indeed, this allows the elastic solution to be used without correction, or require the minimum amount of correction by the method proposed here.
- Though based on the assumption of uniform stress, the possibility of applying the proposed procedure at different depths can give indications about the not yet solved problem of high residual stress with depth gradient.

## Acknowledgments

The authors are grateful to Eng. Andrea Rossi for his valuable contribution in preparing the models and elaborating the finite element results. The SINT Technology company is also acknowledged for financial and technical support and useful discussions.

## References

- [1] *Standard Test Method for Determining Residual Stresses by the Hole–Drilling Strain–Gage Method*, 2008. ASTM E837-08.
- [2] M. Steinzig and E. Ponslet. Residual Stress Measurement using the Hole Drilling Method and Laser Speckle Interferometry: Part I. *Experimental Techniques*, 27(3):43–46, 2003.
- [3] M. Ya, F. Dai, H. Xie, and J. Lü. Measurement of non-uniform residual stresses by combined Moiré interferometry and hole-drilling method: Theory, experimental method and applications. *Acta Mechanica Sinica*, 19(6):567–574, 2003.
- [4] M. Ya, F.L. Dai, H.M. Xie, and J. Lu. Measurement of non-uniform residual stresses by combined Moiré interferometry and hole-drilling method: Theory, experimental method and applications. *ACTA MECHANICA SINICA*, 19(6):567–574, 2003.
- [5] M. Ya, P. Marquette, F. Belahcene, and J. Lu. Residual stresses in laser welded aluminium plate by use of ultrasonic and optical methods. *Materials Science and Engineering A*, 382(1–2):257–264, 2004.
- [6] P.V. Grant, P.D. Lord, and P.S. Whitehead. *The measurement of residual stresses by the incremental hole drilling technique*. National Physical Laboratory, 2002. Measurement good practice guide 53.
- [7] J. Gibmeier, J.P. Nobre, and B. Scholtes. Residual Stress Determination by the Hole Drilling Method in the Case of Highly Stressed Surface Layers. *Materials Science Research International*, 10(1):21–25, 2004.
- [8] J. Gibmeier, M. Kornmeier, and B. Scholtes. Plastic deformation during application of the hole–drilling method. In *ECRS 5: Proceedings of the fifth european conference on residual stresses*, volume 347–3 of *Materials Science Forum*, pages 131–136, 2000.

- [9] E. Valentini, M. Beghini, L. Bertini, C. Santus, and M. Benedetti. Procedure to perform a validated incremental hole drilling measurement, application to shot peening residual stresses. *Strain*, 2009. In press.
- [10] J.P. Nobre, A.M. Dias, J. Gibmeier, and M. Kornmeier. Local Stress–Ratio Criterion for Incremental Hole–Drilling Measurements of Shot–Peening Stresses. *Journal of Engineering Materials and Technology*, 128(2):193–201, 2006.
- [11] J.P. Nobre, A. Loureiro, A.C. Batista, and A.M. Dias. Evaluation of welding residual stresses using the incremental hole–drilling technique. In *Advanced Materials Forum III, parts 1 and 2*, volume 514–516 of *Materials Science Forum*, pages 768–773, 2006.
- [12] R. Moharami and I. Sattari–Far. Experimental and numerical study of measuring high welding residual stresses by using the blind–hole–drilling technique. *The Journal of Strain Analysis for Engineering Design*, 43(3):141–148, 2008.
- [13] L. Fratini and B. Zuccarello. An analysis of through-thickness residual stresses in aluminium FSW butt joints. *International Journal of Machine Tools and Manufacture*, 46(6):611–619, 2006.
- [14] S.P. Timoshenko and J.N. Goodier. *Theory of Elasticity*. McGraw-Hill, 3rd edition, 1970.
- [15] M. Beghini, L. Bertini, and P. Raffaelli. An Account of Plasticity in the Hole–Drilling Method of Residual Stress Measurement. *The Journal of Strain Analysis for Engineering Design*, 30(3):227–233, 1995.
- [16] M. Beghini, L. Bertini, and P. Raffaelli. Numerical Analysis of Plasticity Effects in the Hole–Drilling Residual Stress Measurement. *Journal of Testing and Evaluation*, 22(6):522–529, 1994.
- [17] M. Beghini and L. Bertini. Recent advances in the hole drilling method for residual stress measurement. *Journal of Materials Engineering and Performance*, 7(2):163–172, 1998.
- [18] Vishay. Strain–Gages Datasheets. <http://www.vishay.com/>.
- [19] HBM. Strain–Gages Datasheets. <http://www.hbm.com/>.
- [20] M. Beghini, L. Bertini, and L. F. Mori. Evaluating non-uniform residual stress by the hole-drilling method with concentric and eccentric holes. Part I: definition and validation of the influence functions. *Strain*, 2009. In Press.
- [21] G.S. Schajer. Application of Finite Element Calculations to Residual stress Measurements. *Journal of Engineering Materials and Technology*, 103(2):157–163, 1981.

## A Tabular results of coefficients

		$Z/D = 0.02$				
		$D_0/D = 0.3$	$D_0/D = 0.35$	$D_0/D = 0.4$	$D_0/D = 0.45$	$D_0/D = 0.5$
ASTM A	<i>a</i>	0.00858	0.01186	0.01596	0.02116	0.02797
	<i>b</i>	0.01604	0.02180	0.02868	0.03699	0.04729
ASTM B	<i>a</i>	0.00909	0.01256	0.01696	0.02250	0.02984
	<i>b</i>	0.01776	0.02407	0.03164	0.04066	0.05189
HBM 1	<i>a</i>	0.00875	0.01209	0.01629	0.02155	0.02836
	<i>b</i>	0.01696	0.02302	0.03026	0.03887	0.04935
HBM 2	<i>a</i>	0.00922	0.01272	0.01724	0.02274	0.03010
	<i>b</i>	0.01863	0.02517	0.03317	0.04234	0.05376
HBM 3	<i>a</i>	0.00920	0.01270	0.01722	0.02271	0.03005
	<i>b</i>	0.01858	0.02511	0.03309	0.04225	0.05363

		$Z/D = 0.1$				
		$D_0/D = 0.3$	$D_0/D = 0.35$	$D_0/D = 0.4$	$D_0/D = 0.45$	$D_0/D = 0.5$
ASTM A	<i>a</i>	0.0589	0.0806	0.1069	0.1389	0.1779
	<i>b</i>	0.1147	0.1536	0.1985	0.2509	0.3116
ASTM B	<i>a</i>	0.0622	0.0852	0.1132	0.1470	0.1886
	<i>b</i>	0.1274	0.1702	0.2199	0.2767	0.3426
HBM 1	<i>a</i>	0.0601	0.0824	0.1095	0.1421	0.1817
	<i>b</i>	0.1220	0.1632	0.2110	0.2661	0.3291
HBM 2	<i>a</i>	0.0632	0.0865	0.1155	0.1495	0.1916
	<i>b</i>	0.1344	0.1791	0.2319	0.2908	0.3588
HBM 3	<i>a</i>	0.0631	0.0864	0.1153	0.1493	0.1913
	<i>b</i>	0.1340	0.1787	0.2314	0.2902	0.3580

		$Z/D = 0.2$				
		$D_0/D = 0.3$	$D_0/D = 0.35$	$D_0/D = 0.4$	$D_0/D = 0.45$	$D_0/D = 0.5$
ASTM A	<i>a</i>	0.1011	0.1368	0.1773	0.2232	0.2739
	<i>b</i>	0.2188	0.2888	0.3643	0.4453	0.5290
ASTM B	<i>a</i>	0.1062	0.1437	0.1864	0.2343	0.2874
	<i>b</i>	0.2433	0.3202	0.4029	0.4903	0.5793
HBM 1	<i>a</i>	0.1037	0.1405	0.1824	0.2299	0.2819
	<i>b</i>	0.2346	0.3095	0.3905	0.4772	0.5650
HBM 2	<i>a</i>	0.1085	0.1467	0.1910	0.2402	0.2943
	<i>b</i>	0.2585	0.3397	0.4283	0.5206	0.6131
HBM 3	<i>a</i>	0.1084	0.1466	0.1907	0.2399	0.2939
	<i>b</i>	0.2579	0.3388	0.4273	0.5195	0.6118

		$Z/D = 0.4$				
		$D_0/D = 0.3$	$D_0/D = 0.35$	$D_0/D = 0.4$	$D_0/D = 0.45$	$D_0/D = 0.5$
ASTM A	<i>a</i>	0.1108	0.1487	0.1907	0.2370	0.2873
	<i>b</i>	0.2838	0.3706	0.4598	0.5505	0.6385
ASTM B	<i>a</i>	0.1160	0.1558	0.1998	0.2483	0.3010
	<i>b</i>	0.3172	0.4130	0.5109	0.6090	0.7026
HBM 1	<i>a</i>	0.1141	0.1531	0.1966	0.2445	0.2959
	<i>b</i>	0.3076	0.4010	0.4974	0.5951	0.6875
HBM 2	<i>a</i>	0.1189	0.1595	0.2051	0.2548	0.3085
	<i>b</i>	0.3401	0.4419	0.5472	0.6516	0.7485
HBM 3	<i>a</i>	0.1188	0.1593	0.2049	0.2546	0.3081
	<i>b</i>	0.3392	0.4408	0.5459	0.6500	0.7468

Table 3: Elastic calibration coefficients, different rosettes and hole depths.

$Z/D = 0.02 \quad R = 0.01$

	ASTM A	ASTM B	HBM 1	HBM 2	HBM 3		ASTM A	ASTM B	HBM 1	HBM 2	HBM 3
$w_1$	-4.191	-5.064	-4.657	-5.475	-5.451	$m_1$	-35.36	-40.23	-38.01	-41.69	-41.46
$w_2$	-0.806	-0.712	-0.711	-0.645	-0.646	$m_2$	27.77	28.58	28.08	29.73	29.79
$w_3$	4.086	5.850	5.167	6.760	6.712	$m_3$	51.39	53.32	51.82	49.70	49.79
$w_4$	9.981	8.485	9.383	8.038	8.101	$m_4$	-19.62	-19.11	-17.23	-14.07	-14.84
$w_5$	3.455	4.152	3.886	4.555	4.535	$m_5$	42.31	48.58	46.54	52.28	52.01
$w_6$	0.872	0.701	0.720	0.554	0.558	$m_6$	-13.63	-13.87	-13.79	-14.59	-14.67
$w_7$	-2.346	-3.855	-3.374	-4.754	-4.713	$m_7$	-55.52	-61.24	-59.55	-62.96	-62.85
$w_8$	-11.963	-10.454	-11.265	-9.883	-9.943	$m_8$	3.10	4.60	2.90	2.60	3.17
$w_9$	-0.525	-0.647	-0.609	-0.725	-0.722	$m_9$	-11.18	-12.43	-12.11	-13.29	-13.23
$w_{10}$	-0.203	-0.143	-0.153	-0.093	-0.095	$m_{10}$	-1.81	-1.59	-1.65	-1.35	-1.34
$w_{11}$	-0.175	0.135	0.048	0.326	0.318	$m_{11}$	12.06	13.46	13.18	14.19	14.15
$w_{12}$	4.390	3.993	4.198	3.836	3.850	$m_{12}$	17.86	16.93	17.49	16.92	16.83

$Z/D = 0.02 \quad R = 0.1$

	ASTM A	ASTM B	HBM 1	HBM 2	HBM 3		ASTM A	ASTM B	HBM 1	HBM 2	HBM 3
$w_1$	-2.949	-3.650	-3.366	-4.011	-3.990	$m_1$	-31.83	-35.63	-34.29	-37.08	-36.69
$w_2$	-0.760	-0.705	-0.713	-0.663	-0.664	$m_2$	26.79	26.87	26.37	27.38	27.44
$w_3$	2.838	4.275	3.760	5.043	5.004	$m_3$	48.54	49.43	48.85	46.24	46.19
$w_4$	9.695	8.415	9.226	8.054	8.112	$m_4$	-16.90	-15.73	-13.94	-10.45	-11.25
$w_5$	2.363	2.931	2.748	3.276	3.259	$m_5$	39.47	44.80	43.46	48.30	47.91
$w_6$	0.806	0.679	0.704	0.571	0.574	$m_6$	-12.98	-12.69	-12.59	-12.91	-12.98
$w_7$	-1.398	-2.646	-2.282	-3.402	-3.368	$m_7$	-53.71	-58.33	-57.43	-59.99	-59.79
$w_8$	-11.475	-10.159	-10.901	-9.687	-9.742	$m_8$	-0.01	0.87	-0.76	-1.50	-0.91
$w_9$	-0.293	-0.396	-0.370	-0.463	-0.460	$m_9$	-10.83	-11.90	-11.72	-12.72	-12.64
$w_{10}$	-0.188	-0.138	-0.149	-0.098	-0.099	$m_{10}$	-2.04	-1.90	-1.98	-1.75	-1.74
$w_{11}$	-0.328	-0.063	-0.131	0.100	0.093	$m_{11}$	12.06	13.24	13.11	13.93	13.88
$w_{12}$	4.110	3.753	3.944	3.617	3.631	$m_{12}$	19.02	18.17	18.75	18.24	18.14

$Z/D = 0.02 \quad R = 0.25$

	ASTM A	ASTM B	HBM 1	HBM 2	HBM 3		ASTM A	ASTM B	HBM 1	HBM 2	HBM 3
$w_1$	-1.609	-2.125	-1.932	-2.403	-2.387	$m_1$	-27.32	-29.77	-29.20	-30.90	-30.46
$w_2$	-0.651	-0.607	-0.620	-0.568	-0.567	$m_2$	26.45	25.49	25.40	25.48	25.41
$w_3$	1.434	2.512	2.135	3.098	3.067	$m_3$	44.78	44.48	44.71	41.31	41.05
$w_4$	9.319	8.249	8.946	7.954	8.003	$m_4$	-12.18	-10.36	-8.85	-4.74	-5.89
$w_5$	1.211	1.644	1.514	1.910	1.897	$m_5$	36.34	40.55	39.77	43.62	43.15
$w_6$	0.687	0.585	0.610	0.500	0.501	$m_6$	-12.77	-11.66	-11.89	-11.48	-11.44
$w_7$	-0.381	-1.348	-1.070	-1.933	-1.906	$m_7$	-52.00	-55.45	-55.20	-56.72	-56.34
$w_8$	-10.836	-9.713	-10.365	-9.326	-9.373	$m_8$	-5.92	-5.61	-7.04	-8.45	-7.57
$w_9$	-0.070	-0.155	-0.134	-0.209	-0.207	$m_9$	-10.68	-11.58	-11.49	-12.31	-12.21
$w_{10}$	-0.167	-0.125	-0.134	-0.092	-0.093	$m_{10}$	-2.34	-2.34	-2.35	-2.25	-2.27
$w_{11}$	-0.451	-0.234	-0.290	-0.101	-0.107	$m_{11}$	12.44	13.42	13.41	14.03	13.95
$w_{12}$	3.742	3.427	3.599	3.311	3.323	$m_{12}$	21.46	20.66	21.23	20.80	20.64

Table 4 continued on next page.

$Z/D = 0.1 \quad R = 0.01$

	ASTM A	ASTM B	HBM 1	HBM 2	HBM 3		ASTM A	ASTM B	HBM 1	HBM 2	HBM 3
$w_1$	-4.322	-5.171	-4.957	-5.773	-5.755	$m_1$	5.73	1.23	4.02	-0.33	-0.23
$w_2$	-1.396	-1.294	-1.304	-1.005	-1.014	$m_2$	15.08	17.79	16.30	20.62	20.47
$w_3$	3.464	5.118	4.658	6.121	6.090	$m_3$	-11.55	-3.29	-7.58	-0.38	-0.55
$w_4$	2.804	1.894	2.250	1.273	1.302	$m_4$	-3.59	-8.92	-7.17	-13.47	-13.28
$w_5$	4.010	4.642	4.528	5.134	5.120	$m_5$	-7.93	-4.64	-6.31	-3.54	-3.60
$w_6$	1.765	1.612	1.648	1.295	1.306	$m_6$	-8.40	-10.28	-9.34	-12.58	-12.47
$w_7$	-3.079	-4.462	-4.124	-5.340	-5.313	$m_7$	16.34	9.47	12.40	6.90	7.01
$w_8$	-4.039	-3.130	-3.449	-2.463	-2.493	$m_8$	1.37	6.31	4.79	10.45	10.29
$w_9$	-0.872	-0.947	-0.946	-1.013	-1.011	$m_9$	1.83	1.16	1.43	0.91	0.92
$w_{10}$	-0.487	-0.433	-0.451	-0.349	-0.352	$m_{10}$	0.09	0.41	0.25	0.87	0.85
$w_{11}$	0.563	0.804	0.752	0.952	0.948	$m_{11}$	-4.74	-3.24	-3.78	-2.63	-2.65
$w_{12}$	1.659	1.431	1.514	1.271	1.278	$m_{12}$	6.39	5.27	5.62	4.37	4.40

$Z/D = 0.1 \quad R = 0.1$

	ASTM A	ASTM B	HBM 1	HBM 2	HBM 3		ASTM A	ASTM B	HBM 1	HBM 2	HBM 3
$w_1$	-2.006	-2.664	-2.447	-3.123	-3.107	$m_1$	-2.36	-5.38	-2.94	-6.17	-6.09
$w_2$	-1.271	-1.253	-1.262	-1.069	-1.079	$m_2$	9.61	11.71	10.42	14.40	14.22
$w_3$	1.541	2.826	2.425	3.600	3.573	$m_3$	-2.94	3.57	-0.21	5.65	5.50
$w_4$	2.446	1.767	2.056	1.324	1.349	$m_4$	0.90	-3.91	-2.30	-8.23	-8.02
$w_5$	1.967	2.481	2.343	2.868	2.855	$m_5$	-1.10	1.08	-0.39	1.62	1.58
$w_6$	1.467	1.394	1.425	1.191	1.201	$m_6$	-4.33	-5.75	-4.94	-7.84	-7.71
$w_7$	-1.400	-2.500	-2.193	-3.188	-3.165	$m_7$	9.20	3.69	6.28	1.73	1.84
$w_8$	-3.409	-2.724	-2.981	-2.248	-2.272	$m_8$	-2.23	2.23	0.83	6.04	5.87
$w_9$	-0.417	-0.487	-0.473	-0.542	-0.541	$m_9$	0.59	0.09	0.35	-0.08	-0.07
$w_{10}$	-0.381	-0.345	-0.360	-0.288	-0.291	$m_{10}$	-0.67	-0.41	-0.56	0.00	-0.02
$w_{11}$	0.201	0.402	0.349	0.522	0.518	$m_{11}$	-3.41	-2.13	-2.63	-1.62	-1.65
$w_{12}$	1.374	1.197	1.265	1.081	1.087	$m_{12}$	6.93	5.89	6.22	5.07	5.11

$Z/D = 0.1 \quad R = 0.25$

	ASTM A	ASTM B	HBM 1	HBM 2	HBM 3		ASTM A	ASTM B	HBM 1	HBM 2	HBM 3
$w_1$	-1.541	-1.984	-1.820	-2.291	-2.278	$m_1$	-1.46	-3.94	-1.55	-4.16	-4.09
$w_2$	-0.903	-0.942	-0.935	-0.861	-0.866	$m_2$	7.60	9.26	8.13	11.52	11.37
$w_3$	1.190	2.082	1.791	2.617	2.595	$m_3$	-4.05	1.68	-1.85	3.24	3.10
$w_4$	1.891	1.435	1.639	1.162	1.179	$m_4$	3.28	-1.16	0.33	-5.05	-4.86
$w_5$	1.436	1.795	1.684	2.059	2.049	$m_5$	-2.10	-0.35	-1.83	-0.27	-0.31
$w_6$	1.012	1.002	1.014	0.903	0.908	$m_6$	-3.06	-4.17	-3.45	-5.88	-5.77
$w_7$	-1.008	-1.787	-1.559	-2.268	-2.249	$m_7$	10.47	5.64	8.07	4.15	4.25
$w_8$	-2.595	-2.128	-2.311	-1.830	-1.846	$m_8$	-4.19	-0.06	-1.39	3.32	3.16
$w_9$	-0.274	-0.328	-0.314	-0.368	-0.366	$m_9$	0.97	0.54	0.80	0.44	0.45
$w_{10}$	-0.255	-0.236	-0.245	-0.204	-0.206	$m_{10}$	-0.88	-0.67	-0.80	-0.33	-0.35
$w_{11}$	0.107	0.256	0.214	0.342	0.339	$m_{11}$	-3.85	-2.69	-3.17	-2.26	-2.28
$w_{12}$	1.035	0.911	0.960	0.835	0.839	$m_{12}$	7.23	6.25	6.57	5.51	5.55

Table 4 continued on next page.



$Z/D = 0.2 \quad R = 0.01$

	ASTM A	ASTM B	HBM 1	HBM 2	HBM 3		ASTM A	ASTM B	HBM 1	HBM 2	HBM 3
$w_1$	-3.758	-4.157	-4.224	-4.676	-4.659	$m_1$	-30.41	-34.62	-35.17	-41.37	-41.15
$w_2$	-0.022	-0.007	-0.129	-0.024	-0.032	$m_2$	26.25	25.88	25.07	24.06	24.07
$w_3$	3.215	4.350	4.084	5.233	5.199	$m_3$	11.41	20.15	18.25	30.99	30.57
$w_4$	3.770	3.136	3.406	2.691	2.715	$m_4$	4.03	0.45	2.80	-3.05	-2.83
$w_5$	3.523	3.753	3.858	4.098	4.087	$m_5$	15.86	17.31	18.35	20.52	20.44
$w_6$	0.502	0.459	0.555	0.406	0.415	$m_6$	-18.71	-18.24	-17.85	-17.07	-17.08
$w_7$	-3.424	-4.393	-4.201	-5.123	-5.097	$m_7$	-0.08	-6.11	-4.98	-12.97	-12.71
$w_8$	-4.583	-3.867	-4.135	-3.352	-3.377	$m_8$	-3.24	0.73	-1.31	4.24	4.05
$w_9$	-0.862	-0.852	-0.888	-0.872	-0.872	$m_9$	-1.73	-1.98	-2.18	-2.45	-2.44
$w_{10}$	-0.180	-0.150	-0.174	-0.116	-0.118	$m_{10}$	2.99	2.80	2.76	2.58	2.58
$w_{11}$	0.978	1.142	1.116	1.254	1.250	$m_{11}$	-2.61	-1.22	-1.48	0.08	0.04
$w_{12}$	1.579	1.379	1.452	1.242	1.248	$m_{12}$	5.06	4.08	4.51	3.27	3.31

$Z/D = 0.2 \quad R = 0.1$

	ASTM A	ASTM B	HBM 1	HBM 2	HBM 3		ASTM A	ASTM B	HBM 1	HBM 2	HBM 3
$w_1$	-2.317	-2.682	-2.743	-3.073	-3.062	$m_1$	-5.92	-9.62	-10.71	-14.86	-14.71
$w_2$	-0.027	-0.112	-0.197	-0.177	-0.184	$m_2$	16.88	17.16	16.18	16.33	16.28
$w_3$	1.752	2.747	2.525	3.420	3.396	$m_3$	-9.21	-0.59	-2.14	8.38	8.05
$w_4$	2.839	2.371	2.575	2.052	2.071	$m_4$	7.39	2.80	5.30	-1.23	-0.98
$w_5$	2.202	2.470	2.545	2.757	2.750	$m_5$	-3.11	-1.48	-0.20	1.06	1.01
$w_6$	0.339	0.385	0.452	0.395	0.402	$m_6$	-11.79	-11.71	-11.18	-11.16	-11.12
$w_7$	-2.050	-2.939	-2.764	-3.526	-3.506	$m_7$	16.56	10.04	11.06	4.09	4.30
$w_8$	-3.511	-2.980	-3.184	-2.613	-2.633	$m_8$	-6.60	-1.98	-4.11	1.80	1.59
$w_9$	-0.539	-0.557	-0.582	-0.584	-0.584	$m_9$	2.00	1.64	1.42	1.22	1.23
$w_{10}$	-0.112	-0.102	-0.120	-0.086	-0.088	$m_{10}$	1.68	1.57	1.50	1.45	1.45
$w_{11}$	0.636	0.800	0.771	0.898	0.895	$m_{11}$	-5.95	-4.39	-4.65	-3.18	-3.22
$w_{12}$	1.232	1.079	1.135	0.979	0.984	$m_{12}$	5.72	4.61	5.06	3.76	3.80

$Z/D = 0.2 \quad R = 0.25$

	ASTM A	ASTM B	HBM 1	HBM 2	HBM 3		ASTM A	ASTM B	HBM 1	HBM 2	HBM 3
$w_1$	-1.101	-1.418	-1.428	-1.726	-1.717	$m_1$	-8.58	-13.09	-13.92	-19.11	-18.94
$w_2$	-0.125	-0.198	-0.271	-0.272	-0.276	$m_2$	14.80	14.50	13.62	13.36	13.35
$w_3$	0.770	1.552	1.359	2.059	2.041	$m_3$	-4.55	4.70	3.16	14.04	13.71
$w_4$	2.173	1.836	1.982	1.627	1.639	$m_4$	8.01	4.15	6.25	0.97	1.17
$w_5$	1.108	1.360	1.382	1.599	1.593	$m_5$	0.10	2.45	3.50	5.73	5.67
$w_6$	0.283	0.328	0.388	0.366	0.369	$m_6$	-10.53	-10.02	-9.52	-9.17	-9.16
$w_7$	-1.059	-1.767	-1.609	-2.217	-2.201	$m_7$	12.03	4.99	6.02	-1.34	-1.12
$w_8$	-2.632	-2.257	-2.403	-2.020	-2.033	$m_8$	-7.34	-3.39	-5.21	-0.36	-0.54
$w_9$	-0.274	-0.304	-0.314	-0.334	-0.334	$m_9$	1.29	0.79	0.61	0.22	0.23
$w_{10}$	-0.071	-0.066	-0.082	-0.061	-0.062	$m_{10}$	1.45	1.27	1.19	1.09	1.09
$w_{11}$	0.359	0.497	0.469	0.577	0.575	$m_{11}$	-4.99	-3.33	-3.59	-2.05	-2.09
$w_{12}$	0.908	0.800	0.840	0.734	0.737	$m_{12}$	5.81	4.83	5.23	4.12	4.16

Table 4 continued on next page.

$Z/D = 0.4 \quad R = 0.01$

	ASTM A	ASTM B	HBM 1	HBM 2	HBM 3		ASTM A	ASTM B	HBM 1	HBM 2	HBM 3
$w_1$	-1.579	-1.604	-1.750	-1.567	-1.568	$m_1$	6.11	6.91	6.52	9.38	9.30
$w_2$	1.636	1.847	1.753	1.704	1.706	$m_2$	16.56	22.63	22.18	20.11	20.30
$w_3$	0.348	0.783	0.690	1.246	1.223	$m_3$	-20.14	-25.83	-26.06	-23.21	-23.49
$w_4$	4.662	4.017	4.355	3.619	3.644	$m_4$	11.99	10.26	11.97	7.10	7.31
$w_5$	1.950	1.924	2.020	1.786	1.788	$m_5$	-12.47	-12.63	-12.58	-15.59	-15.51
$w_6$	-0.569	-0.733	-0.706	-0.677	-0.678	$m_6$	-8.93	-14.37	-14.04	-12.89	-13.02
$w_7$	-1.383	-1.904	-1.784	-2.324	-2.303	$m_7$	21.64	25.41	25.84	24.22	24.41
$w_8$	-5.469	-4.673	-4.997	-4.162	-4.188	$m_8$	-11.04	-8.47	-9.97	-5.37	-5.56
$w_9$	-0.841	-0.778	-0.803	-0.695	-0.697	$m_9$	2.93	2.64	2.74	3.15	3.14
$w_{10}$	-0.042	0.013	0.008	0.032	0.031	$m_{10}$	1.43	2.42	2.38	2.10	2.12
$w_{11}$	0.965	1.060	1.039	1.119	1.116	$m_{11}$	-5.88	-6.02	-6.26	-5.57	-5.61
$w_{12}$	1.846	1.602	1.686	1.445	1.452	$m_{12}$	5.81	5.07	5.40	4.35	4.39

$Z/D = 0.4 \quad R = 0.1$

	ASTM A	ASTM B	HBM 1	HBM 2	HBM 3		ASTM A	ASTM B	HBM 1	HBM 2	HBM 3
$w_1$	0.494	0.357	0.196	0.295	0.297	$m_1$	13.01	12.18	11.60	14.90	14.84
$w_2$	1.539	1.592	1.521	1.396	1.398	$m_2$	17.08	22.05	22.02	18.90	19.07
$w_3$	-1.437	-0.836	-0.929	-0.354	-0.375	$m_3$	-26.95	-28.67	-29.66	-25.81	-26.10
$w_4$	3.280	2.759	3.033	2.474	2.494	$m_4$	10.26	7.39	9.39	4.56	4.77
$w_5$	-0.015	0.090	0.190	0.067	0.067	$m_5$	-16.43	-15.55	-15.26	-18.63	-18.56
$w_6$	-0.746	-0.773	-0.756	-0.654	-0.655	$m_6$	-10.54	-14.76	-14.83	-12.58	-12.70
$w_7$	0.442	-0.202	-0.084	-0.637	-0.619	$m_7$	26.63	27.29	28.27	25.68	25.88
$w_8$	-3.933	-3.312	-3.572	-2.946	-2.966	$m_8$	-9.61	-6.31	-8.00	-3.50	-3.68
$w_9$	-0.279	-0.264	-0.285	-0.220	-0.222	$m_9$	3.69	3.27	3.31	3.83	3.81
$w_{10}$	0.053	0.076	0.073	0.076	0.075	$m_{10}$	1.76	2.48	2.52	2.01	2.03
$w_{11}$	0.401	0.530	0.507	0.602	0.599	$m_{11}$	-6.78	-6.38	-6.70	-5.85	-5.89
$w_{12}$	1.361	1.173	1.239	1.058	1.064	$m_{12}$	5.37	4.51	4.87	3.84	3.88

$Z/D = 0.4 \quad R = 0.25$

	ASTM A	ASTM B	HBM 1	HBM 2	HBM 3		ASTM A	ASTM B	HBM 1	HBM 2	HBM 3
$w_1$	0.773	0.575	0.432	0.411	0.413	$m_1$	8.74	6.15	5.40	6.75	6.73
$w_2$	1.015	1.022	0.954	0.841	0.843	$m_2$	14.63	19.02	18.99	15.93	16.09
$w_3$	-1.499	-0.927	-0.996	-0.462	-0.478	$m_3$	-20.56	-19.96	-20.98	-15.58	-15.88
$w_4$	2.323	1.961	2.161	1.782	1.795	$m_4$	10.59	8.00	9.88	5.81	5.99
$w_5$	-0.470	-0.292	-0.206	-0.200	-0.201	$m_5$	-13.21	-10.95	-10.55	-12.25	-12.20
$w_6$	-0.517	-0.506	-0.482	-0.382	-0.384	$m_6$	-8.76	-12.47	-12.55	-10.29	-10.41
$w_7$	0.833	0.238	0.330	-0.182	-0.167	$m_7$	22.23	21.08	22.09	18.11	18.32
$w_8$	-2.764	-2.338	-2.526	-2.104	-2.118	$m_8$	-10.38	-7.35	-8.96	-5.04	-5.20
$w_9$	-0.054	-0.072	-0.087	-0.066	-0.067	$m_9$	3.31	2.65	2.67	2.86	2.85
$w_{10}$	0.053	0.063	0.059	0.055	0.055	$m_{10}$	1.34	1.96	2.01	1.50	1.52
$w_{11}$	0.131	0.258	0.238	0.336	0.333	$m_{11}$	-6.19	-5.46	-5.78	-4.66	-4.71
$w_{12}$	0.953	0.823	0.871	0.747	0.751	$m_{12}$	5.54	4.72	5.08	4.15	4.18

Table 4: Fit function coefficients:  $w_i, m_i (i = 1 \dots 12)$ , different rosettes, strain hardening ratios, and hole depths.

## B Newton–Raphson algorithm to find the plasticity factor

In order to numerically solve Equation 7 to obtain the actual plasticity factor  $f$  when the elastically calculated plasticity factor  $f_{el}$  is known, the Newton–Raphson algorithm was found to be efficiently convergent, when properly adapted to the problem. In the following some useful suggestions are provided for the practical solution of this problem. By assuming that the quantities  $W, \mu$  are known, the following algorithm produces a convergent sequence of approximations of the (actual) plasticity factor  $f$ :

$$\begin{aligned} \hat{f}_1 &= \min\{1, f_{el}\} \\ \hat{f}_{i+1} &= \hat{f}_i - \frac{W\hat{f}_i^\mu + \hat{f}_i - f_{el}}{\mu W\hat{f}_i^{\mu-1} + 1} \end{aligned} \quad (12)$$

It was verified that, with the here suggested initial value, the error  $|\hat{f}_i - f|/f$  is always below 1% when  $i \geq 5$ , thus, for practical applications it can be assumed that:

$$\hat{f} = \hat{f}_5 \quad (13)$$

A different initial value can require a larger number of iterations to reach a numerical solution  $\hat{f}$  having similar precision.

Figures in colors for the on–line version of the paper.

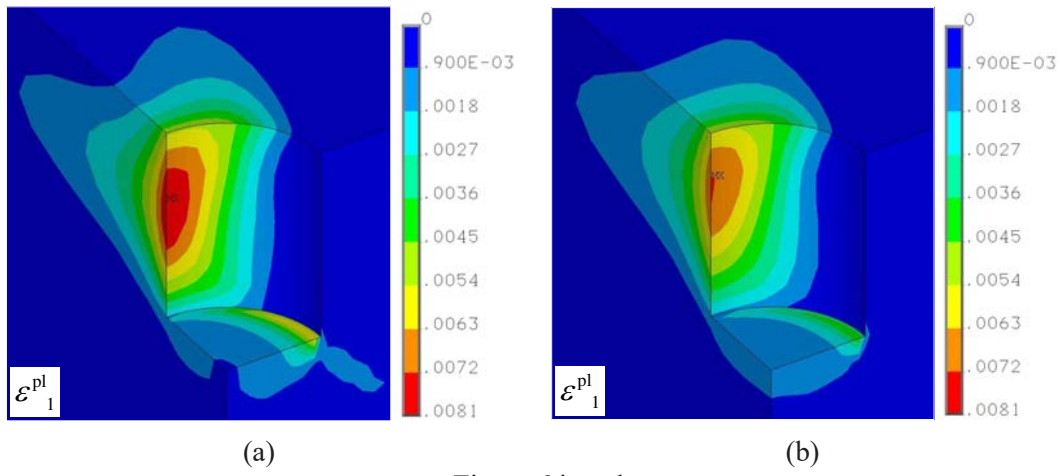


Figure 6 in colors.

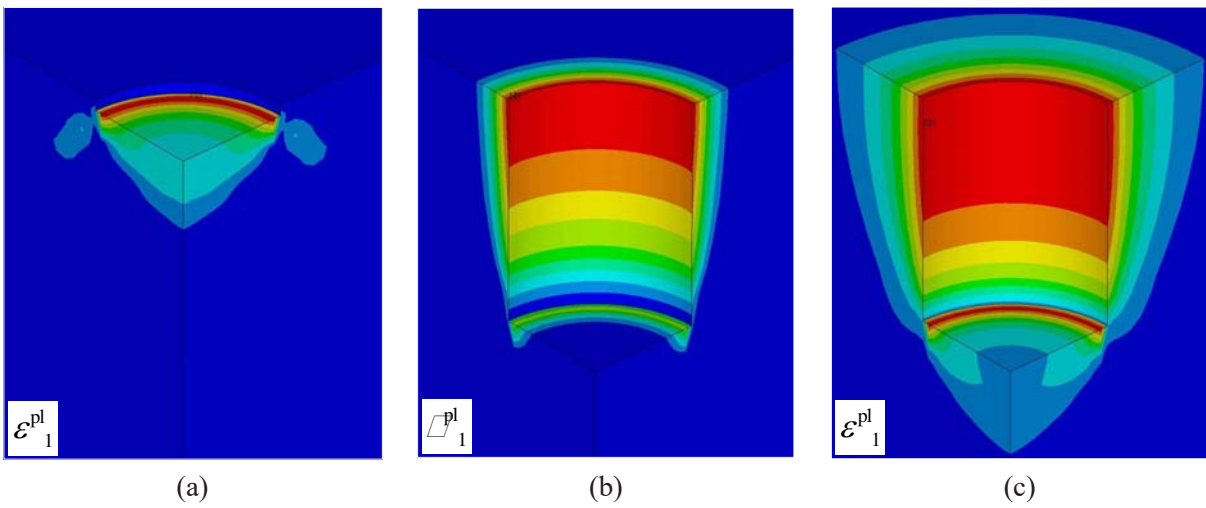


Figure 8 in colors.

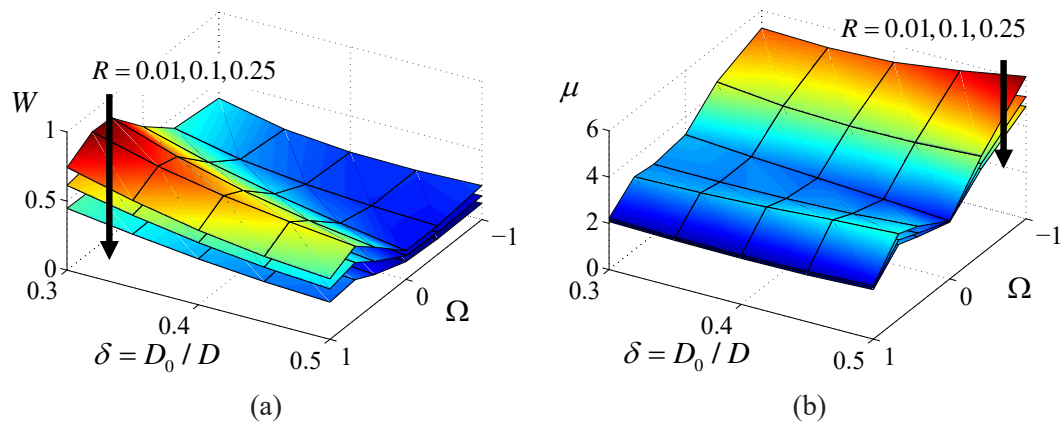


Figure 10 in colors.